

## Effect of Precursors on the Growth and Physiochemical Properties of Bio-mimetic ZnFe<sub>2</sub>O<sub>4</sub> Nanocomposites for Photoelectrochemical Application

(Kesan Prekursor terhadap Pertumbuhan dan Sifat Fisiokimia Nanokomposit ZnFe<sub>2</sub>O<sub>4</sub> Bio-mimetik untuk Aplikasi Fotoelektrokimia)

MOHD FAIZAL MD NASIR, WAN RAMLI WAN DAUD, MOHAMAD AZUWA MOHAMED, MOHAMAD HAFIZ MAMAT, SAIFOLLAH ABDULLAH & MOHAMAD RUSOP MAHMOOD\*

### ABSTRACT

Zinc ferrite (ZnFe<sub>2</sub>O<sub>4</sub>) photocatalysts have been prepared with different types of zinc precursors using the bio-mimetic synthesis method. The kapok fibre (Ceiba pentandra (L.) Gaertn) used as a sacrificial template. The physiochemical of prepared bio-mimetic materials were carried out thoroughly in this work. The FESEM analysis in mimetic zinc ferrite catalysts shows a distinctly different structural transition under different precursors conditions. The acetate precursor formed a hollow tubular structure while other precursors formed a hierarchal fibril structure. X-ray diffraction analysis showed a distinctly different phase transition while UV-Vis spectroscopy recorded variable optical properties beneath different precursor conditions. The EDX and ATR-FTIR spectroscopy confirmed the formation of the pure composite after the annealing process. Different type of precursors that used have leads to tuneable of the magnetic properties of the prepared materials. Electrophoretic deposition (EPD) method has been used to fabricate the synthesized materials as photo-electrodes on the FTO substrate then evaluated for photoelectrochemical (PEC) application. Changing the precursors in the preparation method show a significant effect on physicochemical and PEC performance. The morphology and surface structure of the prepared catalysts are correlated with the alteration of the precursors, then attributed to the charge transfer properties of the photocurrent density in PEC system. The bio-templated zinc ferrite catalysts are promising photoanode in the photocatalytic activities. It is interesting to note that the various forms of multi-structure such as hollow fibril core-shell offers an enormous impact in designing active photocatalyst with superior performance.

**Keywords:** Bio-mimetic; kapok fibre; photoelectrochemical; ZnFe<sub>2</sub>O<sub>4</sub>

### ABSTRAK

Pemangkin zink ferit telah berjaya dihasilkan dengan beberapa jenis bahan pemula yang berlainan seperti zink asetat, zink klorida dan zink nitrat terhadap iron nitrat melalui teknik sintesis bio-mimetik. Serat kekabu (Ceiba pentandra (L.) Gaertn) digunakan sebagai bahan templat. Sifat fizikokimia sebatian zink ferit telah berjaya dicirikan sepenuhnya dalam kajian ini. Analisis morfologi (FESEM) menunjukkan perubahan struktur permukaan apabila bahan pemula yang berbeza digunakan. Bahan pemula zink asetat membentuk struktur tiub yang berongga manakala bahan pemula yang lain membentuk sebatian pemangkin yang berstruktur fibril hierarki. Analisis pembelau sinar-X dan spektroskopi UV-Vis masing-masing merekodkan peralihan fasa yang berbeza dan turut mencatatkan sifat optik yang berlainan yang disebabkan oleh pengaruh bahan pemula yang digunakan. Bahan pemula yang berlainan jenis telah didapati memberikan kesan yang signifikan serta turut menala sifat magnet pemangkin yang dihasilkan. Analisis spektroskopi EDX dan ATR-FTIR mengesahkan pembentukan komposit yang tulen selepas proses penyepuhlindapan bahan templat. Sebatian yang telah disintesis berjaya difabrikasi sebagai elektrod atas permukaan substrat FTO dengan menggunakan teknik pemendapan elektroforetik (EPD). Seterusnya, elektrod yang dihasilkan telah diuji dalam aktiviti fotoelektrokimia (PEC). Pengaruh bahan pemula berlainan jenis terhadap sifat fizikokimia dibincangkan dan dihubungkan dalam aplikasi foto-elektrokimia.

**Kata kunci:** Bio-mimetik; fotoelektrokimia; serat kekabu; ZnFe<sub>2</sub>O<sub>4</sub>

### INTRODUCTION

In recent years, nano-material preparation using bio-mimetic synthesis route has proven to offer the benefits

of unique properties, distinctive physicochemical and catalytic enhancement in catalyst performance (Li et al. 2015; Mohamed et al. 2018; Singh & Chakarvarti 2016).

Modification and improvement of nanoparticle surface structure in 3 dimension morphologies have significantly contributed to a remarkable effect in catalyst performance (Shi et al. 2018). Templating technique provides a clear route for patterning inorganic bio-materials to mimetic the characteristics of the natural product (Mohamed et al. 2018). Due to long-term evolutionary development and optimization, bio-materials has displayed numerous unique hierarchically porous built structures (Singh et al. 2018). Naturally, kapok fibres appear as distinctive hollow fibril shape that consists of cellulose and lignin are chemically stable in aqueous solution and can be heated down (Chai et al. 2018). The peculiar morphology of kapok fibre encouraged scientists to use it as a scaffold template to synthesis bio-mimetic photocatalysts to obtain a hollow structure that very beneficial for various application (Li et al. 2015).

The development of renewable fuel from the conversion of solar energy known as photoelectrochemical water splitting (PEC) has so far attracted researchers attention due to rising energy demand and environmental pollution that is creating a crisis (Kim et al. 2015; Luo et al. 2016; Stevanović et al. 2014; Warfsmann et al. 2018; Zhang et al. 2018). Research and development for efficient and low-cost photocatalysts are still ongoing (Feng et al. 2019; Hajibabaei et al. 2018; Zhang et al. 2018). In recent times, the zinc ferrite semiconductor with a variable band energy gap from 1.75 to 2.2 eV has been designed to achieve high photocatalytic efficiency in their activities (Chai et al. 2018; Li et al. 2015; Song et al. 2015). Zinc ferrite is a photo-active material that extensively used as PEC photocatalyst, which displayed unique properties and remarkable performances in the solar fuel system (Kim et al. 2015; Luo et al. 2016; Warfsmann et al. 2018). However, zinc ferrite semiconductor in photoelectrochemical water splitting systems was overwhelmed by several difficulties such as low surface area, less-sensitivity to visible-light harvesting, less efficient in the injection of charge carriers and separation, blockage of the photo-active site and lower interfacial kinetics of light to chemical conversion that contributes to low efficiency and photochemical stability (Cai et al. 2018; Kim et al. 2015; Stevanović et al. 2014; Zhang et al. 2018).

Numerous studies were devoted to enhance zinc ferrite photocatalytic efficiency and absorption/ harvesting ability in visible light thru morphology configuration strategies, such as doping, templating, heterojunction, composite, hybrid microwave annealing, nanostructure modification, thermal deposition and electrospinning techniques (Cai et al. 2018; Kim et al. 2015; Li et al. 2015; Luo et al. 2016; Peeters et al. 2017; Song et al. 2015; Vinosha et al. 2017). In between, the construction of templated  $ZnFe_2O_4$  material has attracted much attention and is more effective due to its success in enhancing visible

light capability and catalytic properties (Cai et al. 2018; Li et al. 2015). Furthermore, the development of hollow structure configuration proved to be a brilliant strategy for the development of catalyst with high photocatalytic activity (Gapusan & Balela 2020; Li et al. 2015; Mohamed et al. 2018). Moreover, hollow structure nanocomposite configuration will provide a large surface interaction then accelerate photo-generated charge transfer in the semiconductor system. To the best of our knowledge, it is hard to find open literature that has been studied about the effect of precursors in bio-mimetic synthesis and fabrication of zinc ferrite photocatalyst using the templating approach that used in the photoelectrochemical activity.

In the present work, kapok fibre is used as a bio-mimetic template to synthesis the zinc ferrite catalysts by using a different type of precursors such as zinc acetate, zinc chloride, and zinc nitrate into iron nitrate hexahydrate. The plausible formation of the prepared materials is proposed. The templated catalysts are fabricated as a photo-electrodes by using electrophoretic deposition (EPD) technique then measure for photoelectrochemical application. The physicochemical properties of the prepared samples were fully carried out by using X-ray diffraction (XRD), attenuated total reflection Fourier transform infrared spectroscopy (ATR-FTIR), field emission scanning electron microscopy (FESEM), energy dispersive X-Ray (EDX), diffuse reflectance spectra (DRS) and vibrating sample magnetometer (VSM) techniques. The effect of precursors of bio-mimetic synthesis on the physicochemical properties and photoelectrochemical performance are investigated.

#### MATERIALS AND EXPERIMENTAL DETAILS

All reagents for the synthesis are analytical grade and used as received from suppliers. Kapok fibre as bio-mimetic template obtained from Perusahaan Bonda, Kuala Kangsar, Perak, Malaysia. Double distilled water used in this experiment.

Pre-treatment of scaffold template. Kapok fibre as a template was manually cleaned and separated from its seed pod. Then, 5 g of kapok fibre was reflux at 100 °C for 2 h in a stock solution of 10 g/L  $NaCl_2$ . The kapok was left cold, collected and washed with distilled water and dried in an electric oven at 80 °C overnight (Gapusan & Balela 2020).

Bio-mimetic synthesis. A 0.25 M zinc (II) acetate dehydrate and 0.25 M iron nitrate hexahydrate were homogenized in 50 mL of water then sonicates for 15 min. Both solutions were mixed and sonicated for 30 min. Afterwards, 0.5 g of kapok added into the mixture solution, then and there continue with sonication sol-gel immersion for 30 min. The inflated/impregnated kapok

collected and dried under ambient conditions for 6 h then transferred in an electric oven for 6 h at 80 °C. The final step accomplished by annealing the product in the furnace at 500 °C for 2 h and pure product of ZFAC sample were produced. Then, other samples prepared by using the zinc chloride and zinc nitrate hexahydrate precursors denoted as ZFCL and ZFNO, respectively.

Fabrication of photo-electrodes. The synthesized materials fabricated as electrodes on the FTO substrate (1.6 × 2.5 cm) using electrophoretic deposition technique in a 30 mL acetone solution. A specific amount of samples were added in acetone solution then sonicated for 5 min with the addition of iodine. The FTO were arranged facing platinum sheet (5 × 5 cm) in range ~10 mm width in a suspension solution. The EPD process performed using 60 V applied voltage at ambient temperature for 5 min for each film. Lastly, the film dried for few hours and annealed at 200 °C for 1 h in the furnace.

Photoelectrochemical measurement. The films were evaluated for their performance in the photoelectrochemical water splitting system. The fabricated films acted as the photo-anode electrode and affixed in a photocell bearing an active area of 1 cm<sup>2</sup> in a three-electrode system PEC system, where platinum is counter and Ag/AgCl in saturated 3 M KCl as a reference electrode. The 0.5 M Na<sub>2</sub>SO<sub>4</sub> electrolyte was used and purge with N<sub>2</sub> for 30 min prior measurements. The PEC analysis was conducted using a linear scan voltammetry function (Ametek Versastat 4) with a scan rate of 0.05 V s<sup>-1</sup> under 100 mW cm<sup>-2</sup> xenon light irradiations. The electrochemical impedance properties were measure in a similar electrolyte solution under a light condition with an AC amplitude of 10 mV and a frequency between 100 kHz and 1 Hz.

#### CHARACTERIZATIONS

The structural properties of the prepared samples characterized by a Field Emission Scanning Electron Microscope (FESEM) (Merlin Supra 55VP) with a platinum coating. The element of compounds was determined using Energy Dispersive X-ray (EDX, Ametek). The X-ray diffraction (XRD) analyses performed using Bruker D8 Advance Quest diffractometer to obtain the crystallinity properties of samples. The infrared spectra were recorded using attenuated total reflectance ATR Nicolet Fourier Transform Infra-red (FTIR) in an analysis range of 400-4000 cm<sup>-1</sup>. The vibrating sample magnetometer (VSM 7407, Lake Shore) performed to measure the magnetic properties of as-synthesized samples at room temperature with a maximum applied magnetic field of 14 kOe. Photoelectrochemical features were measured using the Potentiostat (Ametek Versastat

4). The optical properties of UV-Vis Diffuse Reflectance Spectroscopy (DRS) were determined using a PerkinElmer UV-Vis-NIR spectrophotometer. The energy band gap was obtained from the Kubelka–Munk function plotting through the intercept value of  $(FR \times hv)^2$  vs  $hv$  for direct transitions. Also, the band edge value of the valance ( $E_{VB}$ ) and conduction band ( $E_{CB}$ ) calculated according to the Mulliken electronegativity theory as reported in previous works (Frese 1979; Pritchard & Skinner 1955; Stevanović et al. 2014). The direct energy gap of the materials is elucidated from the direct linear portion of the energy at the X-axis (Vinosha et al. 2017). The conduction band (CB) and valence band (VB) edge positions were determined by the Mulliken electronegativity theory. The valence band ( $E_{VB}$ ) and conduction band ( $E_{CB}$ ) positions were determined by using the following reactions;

$$E_{VB} = X - E_e + 0.5E_g \quad (1)$$

$$E_{CB} = E_{VB} - E_g \quad (2)$$

whereas, the ECB and EVB are the conduction bands (CB) and the valence band (VB) relative to the normal hydrogen electrode (NHE), respectively. X is the electronegativity of the semiconductor; X value for ZnO is 5.92 and for Fe<sub>2</sub>O<sub>3</sub> is 5.83 (Frese 1979; Pritchard & Skinner 1955; Stevanović et al. 2014).  $E_g$  is the photocatalyst band gap, and  $E_e$  is the energy of free electrons (4.5 eV).

## RESULTS AND DISCUSSION

#### SCHEMATIC ILLUSTRATION GROWTH OF BIO-MIMETIC ZINC FERRITE MATERIALS

The schematic illustration of the bio-mimetic synthesis of ZnFe<sub>2</sub>O<sub>4</sub> nanocomposites depicts in Figure 1. The raw and pre-treatment kapok template are prominently containing a massive number of –OH and –COOH groups on their surface (Cai et al. 2018; Mohamed et al. 2018; Song et al. 2015). Therefore, the metal ions such as Zn<sup>2+</sup> and Fe<sup>3+</sup> ions could be homogeneously impregnated and inflated onto the surface of the templates (Singh & Chakarvarti 2016), then formed the chemical bonding between metal ions precursor onto the kapok template (Yang et al. 2018). Through the calcination process at 500 °C, the kapok template was slowly decomposed and removed then consequently successively Zn<sup>2+</sup>/Fe<sup>3+</sup> ions oxidize then crystallize growth to produce the zinc ferrite materials. As illustrated in Figure 1(b)-1(c)), a different type of precursors that used in the preparation method causes the materials to form a different morphology, structure and physicochemical properties (Malinowska et al. 2020).

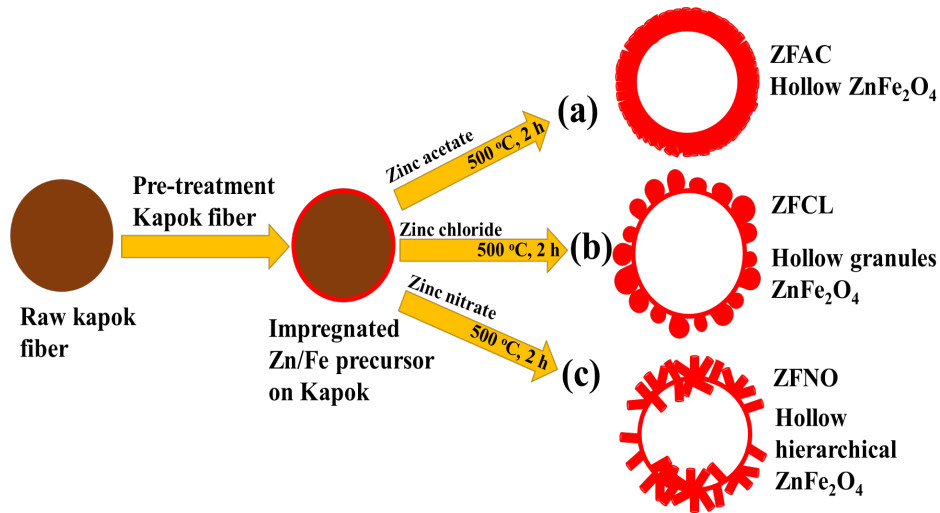


FIGURE 1. Schematic illustration preparation of synthesized zinc ferrite materials

#### STRUCTURAL AND ELEMENTAL ANALYSES

FESEM and EDX images for the synthesized samples depicted in Figure 2. These figures portray the morphology of the prepared samples that successfully mimetic the nature of kapok fibre as collected in Figure 2a(i-ii), 2b(i-ii) and 2c(i-ii), respectively, for namely ZFAC, ZFCL, and ZFNO samples. All materials exhibited a hollow fibril structure of the fibre template. At higher resolution, the ZFAC sample displays a grass wave shape with a uniform vertically align arrangement of fibril nature Figure 2a(ii). Then, the ZFCL sample shows a hollow fibril structure with agglomeration particles on the top of the templated surface, as shown in Figure 2b(i-ii). In contrast, the ZFNO sample depicts a hierarchical morphology with a clear appearance of zinc oxide

nanorod on the hollow fibril  $\text{ZnFe}_2\text{O}_4$  (Figure 2c(ii)). After the formation of the hollow fibril structure ( $\text{ZnFe}_2\text{O}_4$ ), the ZnO rod derives by self-assembly crystallization growth on the C-axis via Oswald ripening after the annealing process (Gapusan & Balela 2020; Yec & Zeng 2014). Significantly, the morphology of the materials was affected by the type of precursors used during coating synthesis (Malinowska et al. 2020). Furthermore, the precursors solution of zinc acetate, zinc chloride, and zinc nitrate formed a different pH value, whereas, the pH value of mixture solution observed during the formation process were 2.34, 2.18, and 2.78, respectively. The different type of precursors with variable values of pH have an impact on the physicochemical properties of the synthesized materials (Malinowska et al. 2020).

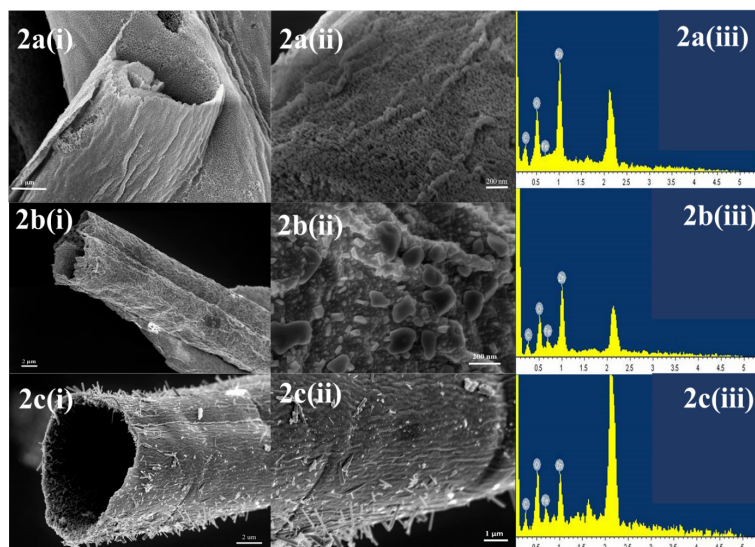


FIGURE 2. The FESEM and EDX images of prepared zinc ferrite samples

## XRD ANALYSIS

The XRD analyses determined the crystalline properties consequently elucidated phase purity of synthesized samples, as depicted in Figure 3(a). This figure illustrates the collected XRD patterns of as-synthesized ZFAC, ZFCL, and ZFNO samples. The ZFAC and ZFCL samples exhibit a cubic (Fd-3m) zinc-iron tetraoxide nanocrystalline phase. While, the ZFNO sample appeared in the mix lattice crystal system and space group of cubic (Fd-3m) consisting of hexagonal (P63mc). The powder data show a good agreement with the JCPDS Card No.; ZFAC: Pdf-01-071-4920, ZFCL: Pdf-01-071-5150 and ZFNO: Pdf-01-071-8731 consisting Pdf-01-071-6424 (zinc oxide rod), respectively. The d-spacing of  $ZnFe_2O_4$  samples was estimated at 0.254 nm (311), respectively, for ZFAC, ZFCL, and ZFNO, while d-spacing for ZnO nanorod on  $ZnFe_2O_4$  of ZFNO sample at 0.247 nm

(101) crystallographic planes. Analyses showed the presence of six diffraction planes for all  $ZnFe_2O_4$  that located at  $2\theta$  angle located at  $\sim 29.9 - 30.09$ ,  $\sim 35.2 - 35.4$ ,  $\sim 42.8 - 43.2$ ,  $\sim 53.1 - 53.3$ ,  $\sim 56.6 - 56.9$ , and  $\sim 62.2 - 62.5$  indexed to the (planes) of (220), (311), (400), (422), (511), and (440), respectively. Then, the patterns corresponding to hexagonal crystal system of ZnO in ZFNO sample exhibited diffraction signals at  $2\theta$  angle of 31.7, 34.4, 36.2, 47.5, 56.6, 62.8 and 67.9 indexed to the (planes) of (100), (002), (101), (102), (110), (103), and (112), respectively. Moreover, the data obtained for all samples are in line with the reported work in Cai et al. (2018) and Li et al. (2015). Importantly, the XRD analyses successfully determined the apparent of  $ZnFe_2O_4$  properties in all samples and formation heterojunction material of ZFNO ( $ZnO/ZnFe_2O_4$ ).

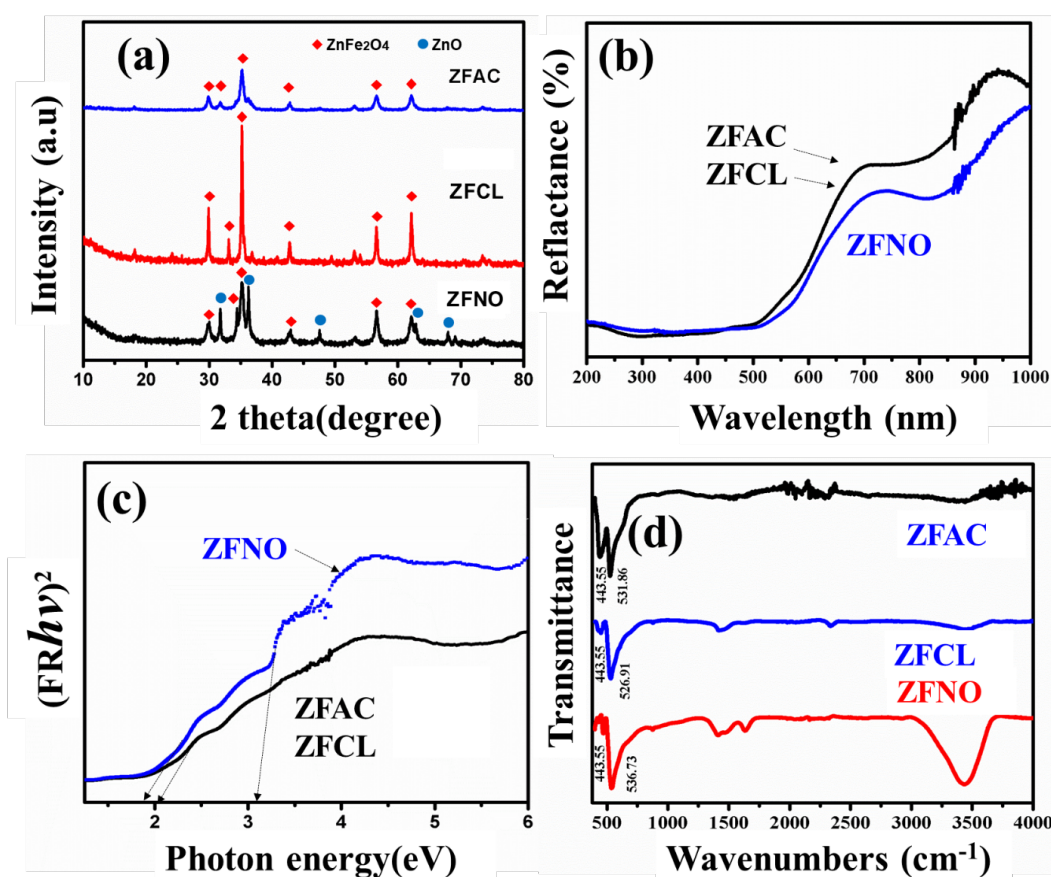


FIGURE 3. The physicochemical results of (a) XRD patterns (b) diffuse reflectance (%R) spectra (c) band gap determination by plot a line at photon energy X-axis and (d) ATR-FTIR for all as-synthesized samples

## UV-VIS SPECTROSCOPY

The UV-Vis. Diffuse reflectance spectra (DRS) analysis were conducted to estimate the band gap ( $E_g$ ), conduction bands ( $E_{CB}$ ), and valence bands ( $E_{VB}$ ) values of the prepared samples. Figure 3(b) shows the diffuse reflectance peaks (%R) of the prepared sample. Whilst the band gap plot are collected in Figure 3(c). The optical properties of prepared samples were collected in Table 1 and the illustration in Figure 4. As seen in Figure 3(b), the value of absorbance edge for ZFNO sample is 725 nm, while the ZFAC and ZFCL exhibit a red-shift of spectral response up to approximately 705 nm. Notably, the analyses recorded

similar band gap patterns in ZFAC and ZFCL samples, while differing in ZFNO, which related to the effect of the precursors. Referring to Figure 2c(i-ii), the type of precursor has altered the morphology of the ZFNO sample to form a hierarchical structure that consists of ZnO rod. As shown in Figure 3(b)-3(c) and illustration in Figure 4, The optical analysis shows a broad absorbance in the diffuse reflectance peaks and extra small peak in band gap plot that identified the appearance of ZnO rod on the surface of ZFNO sample. In the ZFNO sample, the optical properties of the ZnO material are 3.15, 3.00 and -0.16 eV, respectively.

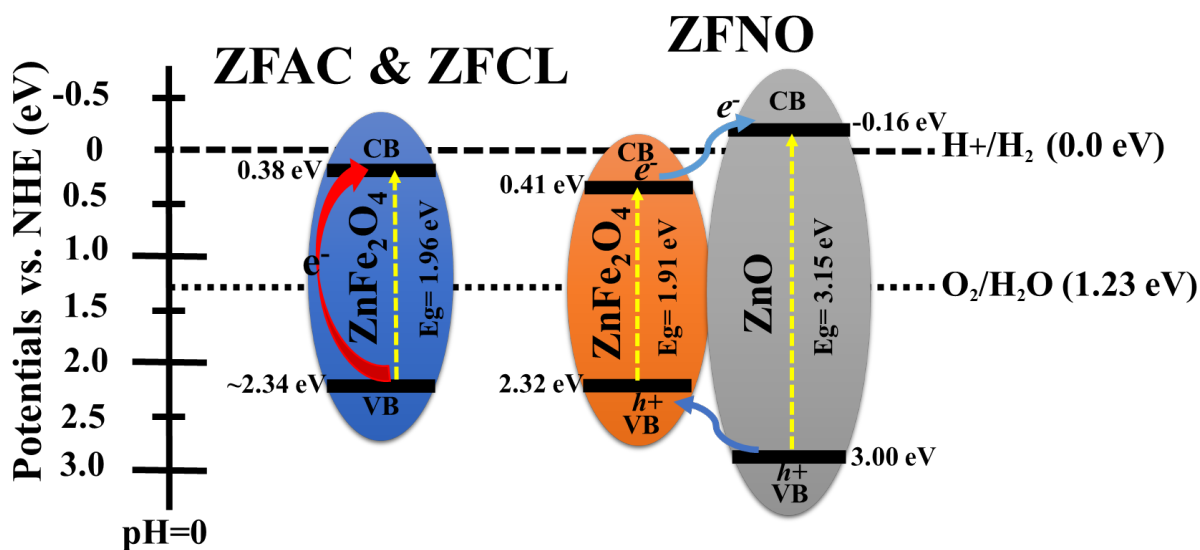


FIGURE 4. The band gap energy and band edge alignment of as-synthesized samples

TABLE 1. Optical properties for prepared samples

Sample / eV	$E_g$	$E_{VB}$	$E_{CB}$
ZFAC	1. 1.96	2. -2.34	3. +0.38
ZFCL	4. 1.96	5. -2.33	6. +0.38
ZFNO/ZnO	7. 1.91 / 3.15	8. -2.32 / -0.16	9. +0.4 / +3.0

## ATR-FTIR SPECTROSCOPY

The Fourier transform infrared (FTIR) spectroscopy was performed to determine the complete removal of wax, cellulose, and other functional groups in the template

that belonging to kapok peaks (Cai et al. 2018; Li et al. 2015; Mohamed et al. 2018; Singh & Chakarvarti 2016). The FTIR analysis showed the complete disappearance of the organic species stretching frequency of the kapok

template at 500 °C (Mohamed et al. 2018). As depict in Figure 3(d), the as-synthesized samples recorded two significant metal stretching bands which assign for ZFAC ( $\nu_1=531.86\text{ cm}^{-1}$ ,  $\nu_2= 443.55\text{ cm}^{-1}$ ), ZFCL ( $\nu_1=526.91\text{ cm}^{-1}$ ,  $\nu_2= 443.55\text{ cm}^{-1}$ ), and ZFNO ( $\nu_1=536.73\text{ cm}^{-1}$ ,  $\nu_2= 443.55\text{ cm}^{-1}$ ). Other peaks are recognized to IR background vibrations that derived from the surrounding environment on the diamond surface, which are carbon dioxide and H-O-H bonds that appeared fingerprint region at 2000 - 2400, 3550 - 3700, and 1610  $\text{cm}^{-1}$ , respectively. Despite that, moisture peaks of OH stretch and O-H-H scissors were recorded in the ZFNO sample at region 3490 and 1610  $\text{cm}^{-1}$ , respectively. It noticed that the zinc nitrate precursor cause the  $\nu_1$  peak to shifted to 536.73  $\text{cm}^{-1}$  that attribute from the hierrichal structure that elongate the Zn-O bond to higher values.

#### MAGNETIC PROPERTIES

The VSM magnetometer used to determine the magnetic properties of the prepared samples, as depicted in Figure

5, which portray the magnetic hysteresis loops of the synthesized materials for ZFAC, ZFCL and ZFNO. The inset shows the magnification near-zero fields. The magnetization properties of prepared samples were summarized in Table 2. As can be seen from the table, the zinc precursors used in the preparation method have a significant effect on magnetization saturation, remanence, and coercivity data. As can be seen in the table, the ZFCL sample shown a higher magnetic properties behaviour compare to other samples as the  $H_c$  and magnetic moment of this sample exhibited a value of 141.9 Gauss and  $0.0254\ \mu_B$ . Also, the retentivity and remanence ratio ( $M_r/M_s$ ) resulted in a higher value in ZFCL material as could be arranged in order of hard > soft; ZFCL > ZFAC > ZFNO, which, indicated a hard behaviour for ZFCL sample that appealing to be used as magnetic recording media devices (Peeters et al. 2017). Significantly, the variation of precursors used in the preparation method leads to tuneable of the magnetic properties of the materials prepared in this work.

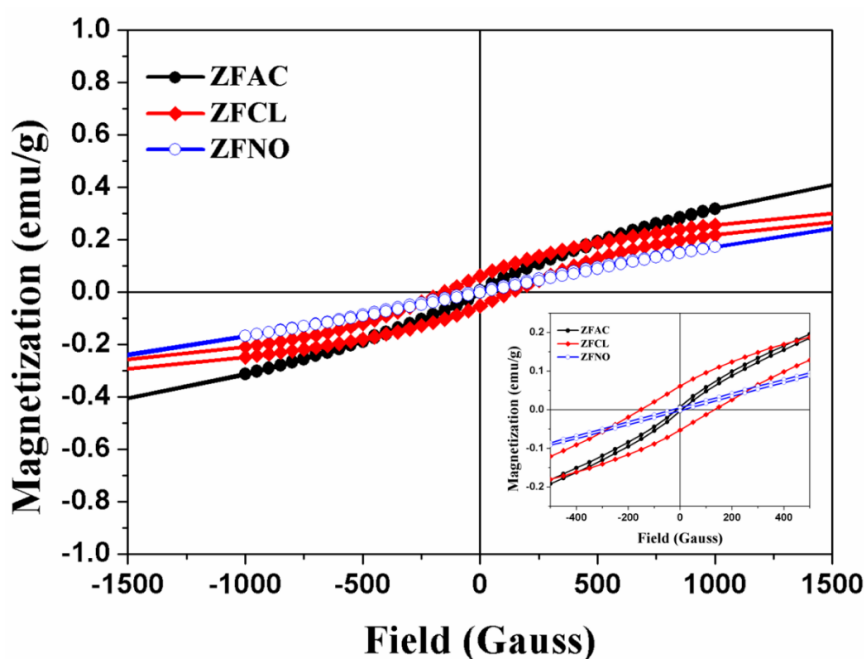


FIGURE 5. Magnetization curves of all samples

TABLE 2. The magnetic properties of synthesized samples

Magnetic properties/ samples	ZFAC	ZFCL	ZFNO
Coercivity, ( $H_{ci}$ ) (G)	7.5312	141.9	21.565
Magnetization, ( $M_s$ ) (emu/g)	1.3845	1.0494	1.8451
Retentivity, ( $M_r$ ) (emu/g)	0.0014	0.0569	0.004
$M_r/M_s$	0.0010	0.0542	0.0022
Magnetic moment ( $\mu_B$ )	0.0018	0.0254	0.0068

## PHOTOELECTROCHEMICAL ACTIVITY

The prepared samples were fabricated as photo-electrodes then measure for photoelectrochemical properties. The electrodes were prepared using a facile electrophoretic deposition (EPD) method. The PEC activity of the ZFAC, ZFCL, and ZFNO photo-electrodes was performed in positive bias potential through a linear scan voltammetry method from 0 to 1.0 V bias potential versus Ag/AgCl in a 0.5 M NaSO<sub>4</sub> electrolytes which executed under one-sun illumination. As can be seen, Figure 6 shows the result of PEC measurements of the bio-templated zinc ferrite materials. The PEC measurement in Figure 6(a)-6(c) shows the effect of precursors on the photocurrent attained. The photocurrent density attained from the prepared samples is 58.5, 33.1, and 6.1  $\mu\text{A cm}^{-2}$  at bias applied 0.7 V, respectively, for ZFAC, ZFCL, and ZFNO electrodes. High photocurrent obtained from ZFAC samples is due to their vertically aligned morphology which suggests to the high surface area leading to improved light scattering, hence highest photocatalytic activity (Ikhmal Salehmin et al. 2019; Kisch 2013). Modify photocatalyst surface structure with a different type of zinc precursor thru bio-template synthesis shown a significant effect on the PEC performance. The photocatalyst containing a uniform hollow vertical-align structure of ZFAC photo-anode exhibited a high current density compare than others is because of their uniform morphology that produces good electron mobility in the PEC system, in addition to a good conductor of magnetic material. Furthermore, the lower band energy gap obtained in ZFAC is beneficial for harvesting properties of PEC activity. Finding in this work shows that the various type of precursors used in

the preparation method alters the catalyst structure, band edge, magnetic properties, and photoelectrochemical performance. Moreover, on the fundamental view, surface structure properties such as a surface topology and surface atomic arrangement play an essential role in effecting the adsorption reaction of reactant for the charge carriers pathways and oxidation reactions mechanisms. Adsorption of water on the surface of the electrode is critical processes that influence the transportation of charge carriers and mechanisms of splitting reactions. Furthermore, water oxidation reaction pathway and rate-determining step depend on the coordination of the atoms on the surface as well as the surface terminal groups (Hajibabaei et al. 2018). The exposure of crystal facet of the semiconductor is the main factor that influences the injection and transportation of charge carrier in the PEC system. The atomic arrangements at different facets would lead to various reaction mechanisms such as crystal facet that expose at (101), (100), and (001) which significantly effect the PEC performance (Kim et al. 2015). Uniform oriented of zinc ferrite semiconductor enhance the separation of charge carriers and promoted an efficient catalytic activity (Luo et al. 2016). Herein, as can be seen in XRD analysis in Figure 2(a), the sample prepared by using zinc nitrate precursor formed a hierarchical structure that results in the mix and dominating phase of (100) peak in result weakening the photocurrent (Kim et al. 2015).

Figure 6(d) portrays the qualitative Nyquist plot of the electrochemical impedance spectra (EIS) evaluation for prepared samples. The smallest diameter of the semicircle as shown in the Nyquist plot indicates the lowest charge-transfer resistance in the order of ZFAC>ZFCL>ZFNO.

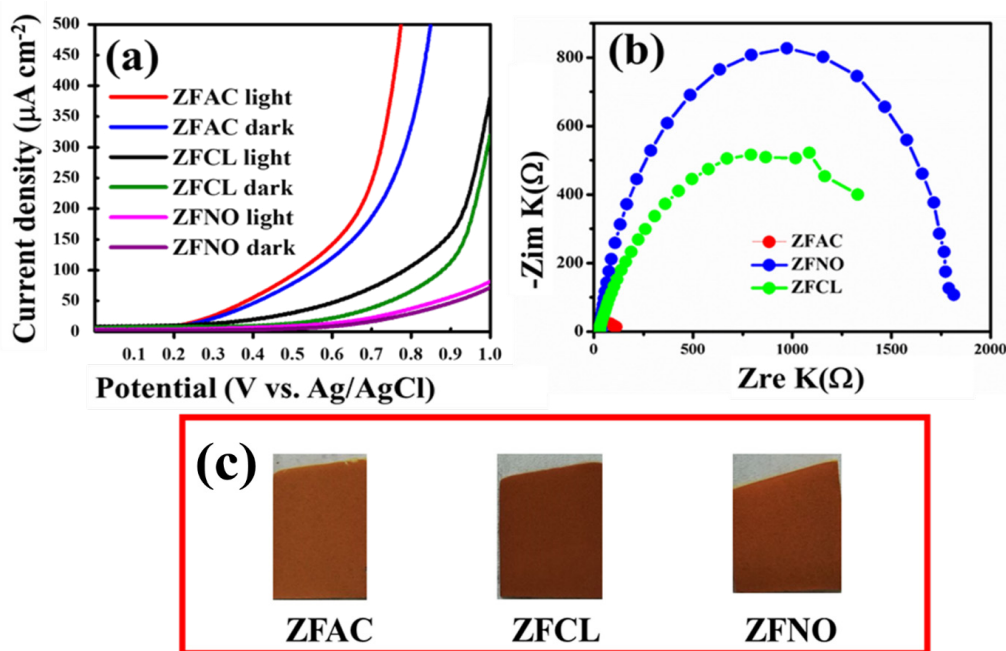


FIGURE 6. (a) PEC analyses (b) Nyquist plot (c) Samples prepared as electrodes

## CONCLUSION

The attained results show a significant influence of a precursors type on the morphology, physicochemical, and magnetic properties of zinc ferrite catalysts that prepared by the bio-mimetic synthesis method. It was found that the photoelectrochemical properties are correlated with the type of precursors which alter the morphology, optical and magnetic properties of the prepared catalyst. The zinc ferrite sample from zinc acetate precursors showed the smaller charge transfer-resistant and the highest current density. The zinc ferrite films exhibited the photocurrent density at range 6 to 58  $\mu\text{Acm}^{-2}$  in 0.5 M  $\text{Na}_2\text{SO}_4$  electrolyte solution at 0.7 V vs. Ag/AgCl under solar AM 1.5 illumination ( $100 \text{ mW cm}^{-2}$ ). This work contributes to the new findings on the effect of precursors in the bio-mimetic synthesis, including pioneer fabrication of bio-mimetic materials through electrophoretic deposition method for PEC activity. The bio-mimetic zinc ferrite photocatalysts were successfully studied in the photoelectrochemical application under the influence of different precursors. In this regard, varying the metal precursors may be regarded as a simple technique to optimize the surface texture, physicochemical, optical as well as the magnetic properties of the templated zinc ferrite catalyst in the photoelectrochemical application.

## ACKNOWLEDGEMENTS

This work was supported by the Ministry of Higher Education (MOHE), Malaysia to Universiti Kebangsaan Malaysia through LRGS/2013/UKM/TP; LRGS/2013/UKM/TP/01 and Universiti Teknologi MARA LRGS/2013/UKM/TP/04. We would like to thank Nano-SciTech Centre-Institute of Science, FSG UiTM, and Fuel Cell Institute UKM for the facilities provided. The manuscript was written through the contributions of all authors. All authors have approved the final version of the manuscript. The authors agreed that there is no competing financial interest.

## REFERENCES

- Cai, A., Guo, A., Du, L., Chang, Y. & Wang, X. 2018. Nanofibrillated cellulose-assisted synthesis of fiber-like ZnO-ZnFe<sub>2</sub>O<sub>4</sub> composites with enhanced visible-light-driven photocatalytic activity. *The Journal of The Minerals, Metals & Materials Society* 70(10): 2169-2172.
- Frese, K.W. 1979. Simple method for estimating energy levels of solids. *Journal of Vacuum Science and Technology* 16(4): 1042-1044.
- Gapusan, R.B. & Mary, D.L.B. 2020. Adsorption of anionic methyl orange dye and lead(II) heavy metal ion by polyaniline-kapok fiber nanocomposite. *Materials Chemistry and Physics* 243: 122682.
- Hajibabaei, H., Gao, Y. & Hamann, T.W. 2018. Chapter 4: Unravelling the charge transfer mechanism in water splitting hematite photoanodes. *RSC Energy and Environment Series* 2018-Janua(20): 100-127.
- Izabela, M., Ryżyńska, Z., Mrotek, E., Klimczuk, T. & Zielińska-Jurek, A. 2020. Synthesis of CoFe<sub>2</sub>O<sub>4</sub> nanoparticles: The effect of ionic strength, concentration, and precursor type on morphology and magnetic properties. *Journal of Nanomaterials* 2020: 1-12.
- Kim, C.W., Yeob, S.J., Cheng, H.M. & Kang, Y.S. 2015. A selectively exposed crystal facet-engineered TiO<sub>2</sub> thin film photoanode for the higher performance of the photoelectrochemical water splitting reaction. *Energy and Environmental Science* 8(12): 3646-3653.
- Kim, J.H., Kim, J.H., Jang, J.W., Kim, J.Y., Choi, S.H., Magesh, G. & Lee, J.S. 2015. Awakening solar water-splitting activity of ZnFe<sub>2</sub>O<sub>4</sub> nanorods by hybrid microwave annealing. *Advanced Energy Materials* 5(6): 1401933.
- Kisch, H. 2013. Semiconductor photocatalysis-mechanistic and synthetic aspects. *Angewandte Chemie - International Edition* 52(3): 812-847.
- Li, J., Ng, D.H.L., Song, P., Song, Y. & Kong, C. 2015. Bio-inspired synthesis and characterization of mesoporous ZnFe<sub>2</sub>O<sub>4</sub> hollow fibers with enhancement of adsorption capacity for acid dye. *Journal of Industrial and Engineering Chemistry* 23(March): 290-298.
- Luo, Z., Li, C., Zhang, D., Wang, T. & Gong, J. 2016. Highly-oriented Fe<sub>2</sub>O<sub>3</sub>/ZnFe<sub>2</sub>O<sub>4</sub> nanocolumnar heterojunction with improved charge separation for photoelectrochemical water oxidation. *Chemical Communications* 52(58): 9013-9015.
- Mohamed, M.A., Zain, M.M.F., Jeffery Minggu, L., Kassim, M.B., Saidina Amin, N.A., Salleh, W.W.N. & Mohd Hir, Z.A. 2018. Constructing bio-templated 3D porous microtubular c-doped g-c<sub>3</sub>n<sub>4</sub> with tunable band structure and enhanced charge carrier separation. *Applied Catalysis B: Environmental* 236: 265-279.
- Peeters, P.D., Taffa, D.H., Kerrigan, M.M., Ney, A., Jöns, N., Rogalla, D. & Devi, A. 2017. Photoactive zinc ferrites fabricated via conventional cvd approach. *ACS Sustainable Chemistry and Engineering* 5(4): 2917-2926.
- Pritchard, H.O. & Skinner, H.A. 1955. The concept of electronegativity. *Chemical Reviews* 55(4): 745-786.
- Salehmin, M.N.I., Jeffery Minggu, L., Arifin, K., Mohamad Yunus, R., Mohamed, M.A. & Kassim, B.M. 2019. Recent advances on state-of-the-art copper (I/II) oxide as photoelectrode for solar green fuel generation: Challenges and mitigation strategies. *Applied Catalysis A: General* 582: 117104.
- Shi, R., Zhang, Y., Wang, X., Ma, Q., Zhang, A. & Yang, P. 2018. Electrospun ZnFe<sub>2</sub>O<sub>4</sub> nanotubes and nanobelts: Morphology evolution, formation mechanism and fenton-like photocatalytic activities. *Materials Chemistry and Physics* 207: 114-122.
- Song, H., Zhu, L., Li, Y., Lou, Z., Xiao, M. & Ye, Z. 2015. Preparation of ZnFe<sub>2</sub>O<sub>4</sub> nanostructures and highly efficient visible-light-driven hydrogen generation with the assistance of nanoheterostructures. *Journal of Materials Chemistry A* 3(16): 8353-8360.
- Stevanović, V., Lany, S., Ginley, D.S., Tumas, W. & Zunger, A. 2014. Assessing capability of semiconductors to split water using ionization potentials and electron affinities only. *Physical Chemistry Chemical Physics* 16(8): 3706-3714.

- Sven, W., Taffa, D.H. & Wark, M. 2018. Photoelectrocatalytic behavior of electrodeposited zinc ferrite films with varying Zn:Fe ratio. *Journal of Photochemistry and Photobiology A: Chemistry* 362: 49-57.
- Varsha, S. & Chakarvarti, S.K. 2016. Biotemplates and their uses in nanomaterials synthesis: A review. *American Journal of Bioengineering and Biotechnology* 2(1): 1-4.
- Vinoshia, P.A., Mely, L.A., Jeronsia, J.E., Krishnan, S. & Jerome, D.S. 2017. Synthesis and properties of spinel ZnFe<sub>2</sub>O<sub>4</sub> nanoparticles by facile co-precipitation route. *Optik* 134: 99-108.
- Yang, X., Han, X., Chen, Z., Zhou, L., Zhao, B., Su, H. & Jiao, W. 2018. Fabrication of Li<sub>7</sub>La<sub>3</sub>Zr<sub>2</sub>O<sub>12</sub> fibers using bio-mass template kapok. *Materials Letters* 217: 271-275.
- Yec, C.C. & Zeng, H.C. 2014. Synthesis of complex nanomaterials via ostwald ripening. *Journal of Materials Chemistry A* 2(14): 4843-4851.
- Zhang, P., Wang, T. & Gong, J. 2018. Current mechanistic understanding of surface reactions over water-splitting photocatalysts. *Chem.* 4(2): 223-245.
- Mohd Faizal Md Nasir & Saifollah Abdullah  
Faculty of Applied Sciences  
Universiti Teknologi MARA  
40450 Shah Alam, Selangor Darul Ehsan  
Malaysia
- Mohd Faizal Md Nasir, Mohamad Hafiz Mamat, Saifollah Abdullah & Mohamad Rusop Mahmood\*  
NANO-SciTech Centre, Institute of Science  
Universiti Teknologi MARA  
40450 Shah Alam, Selangor Darul Ehsan  
Malaysia
- Mohamad Hafiz Mamat & Mohamad Rusop Mahmood\*  
NANO-Electronic Centre  
Faculty of Electrical Engineering  
Universiti Teknologi MARA  
40450 Shah Alam, Selangor Darul Ehsan  
Malaysia
- Mohd Faizal Md Nasir & Wan Ramli Wan Daud  
Fuel Cell Institute (SELFUEL)  
Universiti Kebangsaan Malaysia  
43600 UKM Bangi, Selangor Darul Ehsan  
Malaysia
- Mohamad Azuwa Mohamed  
Centre for Advanced Material and Renewable Resources (CAMARR)  
Faculty of Science and Technology  
Universiti Kebangsaan Malaysia  
43600 UKM Bangi, Selangor Darul Ehsan  
Malaysia
- Wan Ramli Wan Daud  
School of Chemical and Process Engineering  
Faculty of Engineering and Built Environment  
Universiti Kebangsaan Malaysia  
43600 UKM Bangi, Selangor Darul Ehsan  
Malaysia
- \*Corresponding author; email: rusop@uitm.edu.my
- Received: 12 August 2020  
Accepted: 11 September 2020